Precursor Evolution and Nucleation Mechanism of $YBa_2Cu_3O_x$ Films by TFA Metal−Organic Decomposition

J. Gàzquez,[†] F. Sandiumenge,*[,†] M. Coll,[†] A. Pomar,[†] N. Mestres,[†] T. Puig,[†] X. Obradors,[†] Y. Kihn,[‡] M. J. Casanove,[‡] and C. Ballesteros[§]

Institut de Ciència de Materials de Barcelona (CSIC), Campus de la UAB, 08193 Bellaterra, Catalonia, Spain, CEMES, 29, rue Jeanne Marvig, BP 94347, 31055 Toulouse Cedex 4, France, and Universidad Carlos III de Madrid, Avenida de la Universidad, 30, 28911 Leganés, Madrid, Spain

Received July 31, 2006. Revised Manuscript Received October 10, 2006

We describe the conversion of yttrium, barium, and copper trifluoracetate-derived solid precursors to epitaxial $YBa_2Cu_3O_x$ superconducting ceramics on (001)-oriented $LaAlO_3$ substrates. Transmission electron microscopy, electron energy loss spectroscopy, energy-dispersive X-ray analysis, and X-ray diffraction are used to characterize the reaction path and nucleation mechanism yielding high critical current $YBa_2Cu_3O_7$. Our results show that the pyrolysis of the trifluoracetate solutions yields a nanostructured, partially amorphous $Ba_{1-x}Y_xF_{2+x}$ matrix having a Ba/Y ratio close to 2, with homogeneously dispersed CuO nanoparticles. Upon heating, the chemical trajectory of the fluoride matrix and the overall microstructural evolution of the ceramic precursor prior to $YBa_2Cu_3O_7$ nucleation is driven by the decomposition and oxidation of this solid solution. The Y solid solubility decreases with temperature yielding Y_2O_3 which reacts with the CuO particles forming $Y_2Cu_2O_5$ at about 700 °C. In addition, electron energy loss spectroscopy reveals a high oxygen concentration and almost no Y in the matrix quenched from 795 °C, at a stage where the $YBa_2Cu_3O_x$ phase still forms disconnected 50−100 nm thick islands spaced by 1−2 μm. The observed evolution from $Ba_{1-x}Y_xF_{2+x}$ to a barium oxyfluoride mostly occurs prior to the heteroepitaxial nucleation of $YBa_2Cu_3O_x$ at about 700 °C. Hence, a microstructural scenario is defined which favors competitive nucleation growth between heteroepitaxial $YBa_2Cu_3O_x$ and bulk $Y_2Cu_2O_5$. X-ray diffraction pole-figure analysis reveals that the oxyfluoride phase is heavily textured, exhibiting two epitaxial relationships with the (001)-$LaAlO_3$ substrate: (001)OF//(001)$LaAlO_3$, [110]OF//[100]$LaAlO_3$ and (111)OF//(001)$LaAlO_3$, [110]OF//[100]$LaAlO_3$ (OF stands for oxyfluoride). High-resolution observations of the growth front support that (111)-oriented oxyfluoride regions provide low-barrier nucleation sites for *c*-axis-oriented $YBa_2Cu_3O_x$ on the buried (001)-$LaAlO_3$ substrate. However, owing to its high mismatch, this orientation only represents roughly 15% percent of the total OF volume. Considering that the nucleation of $YBa_2Cu_3O_x$ is confined to those regions, this would lead to an anomalously large internuclei spacing, as is indeed observed, favoring the formation of large $YBa_2Cu_3O_x$ grains and films with a low mosaic spread.

Introduction

Growth of $YBa_2Cu_3O_{7-x}$ (YBCO) films by metal−organic decomposition (MOD) using trifluoroacetate (TFA) precursor solutions is attracting much interest owing to its great potential for a cost-effective production of high-performance superconductor tapes, as reviewed by several authors.[1−3] Solution deposition is now an established technique for a number of functional ceramic films.[4−7] However, although high critical currents have already been reported for TFA-derived YBCO, a detailed understanding of the mechanisms controlling the precursor conversion to the final film is still far from being achieved. This knowledge is essential for a reproducible production of long-length tapes exhibiting high mechanical and superconducting performance. TFA precursors were first proposed for the production of YBCO in order to avoid the formation of $BaCO_3$,[8] which requires extreme processing conditions and may result in a significant degradation of the superconducting properties.[9,10] Nominally, during the pyrolysis barium trifluoracetate yields BaF_2, which is subsequently converted to BaO through reaction with H_2O and formation of HF.

Once the precursor solution is deposited on a substrate, either by spin coating or dip coating, growth of films is carried in two steps: First, the organic precursor is decomposed in a pyrolysis step, yielding yttrium, barium, and

* Author to whom correspondence should be addressed.
† Institut de Ciència de Materials de Barcelona.
‡ CEMES.
§ Universidad Carlos III.

(1) Obradors, X.; Puig, T.; Pomar, A.; Sandiumenge, F.; Mestres, N. In *Studies of High Temperature Superconductors*; Narlikar, A. V., Ed.; Nova Science: New York, 2005; Vol. 49, pp 79−123.
(2) Rupich, M. W.; Verebelyi, D. T.; Zhang, W.; Kodenkandath, Th.; Li, X. *MRS Bull.* **2004**, *29*, 572.
(3) Araki, T.; Hirabayashi, I. *Supercond. Sci. Technol.* **2003**, *16*, R71.
(4) Schwartz, R. W.; Schneller, Th.; Waser, R. *C. R. Chim.* **2004**, *7*, 433.
(5) Schwartz, R. W. *Chem. Mater.* **1997**, *9*, 2325.
(6) Scherrer, G. W. *J. Sol.-Gel Sci. Technol.* **1997**, *8*, 353.
(7) Lange, F. F. *Science* **1996**, *273*, 903.
(8) Gupta, A.; Jaganathan, R.; Cooper, E. I.; Giess, E. A. *Appl. Phys. Lett.* **1988**, *52*, 2077.
(9) Parmigiani, F.; Chiarello, G.; Ripamonti, N.; Foretzki, H.; Roll, U. *Phys. Rev. B* **1987**, *36*, 7148.
(10) Hirano, S.; Hayashi, T.; Miura, M. *J. Am. Ceram. Soc.* **1990**, *73*, 885.

10.1021/cm0617891 CCC: $33.50
Published on Web 12/06/2006

copper oxyfluorides,[8,11,12] which are reacted in a subsequent high-temperature process under a water vapor pressure to give YBCO + HF. Various forms of the overall reaction have been proposed in the literature,[1−3] but there is ample evidence that the reaction path to the final epitaxial YBCO film is, however, complex, both chemically and topologically. The growth rate of the YBCO film is governed by T, $P(H_2O)$, and total pressure,[13,14] and it has been demonstrated that a careful adjustment of the process parameters is essential to control the microstructure and therefore the critical currents of the films.[15]

Understanding the conversion mechanism to fully reacted YBCO requires detailed knowledge on the reaction path. Early reports had proposed that as-pyrolyzed materials consist of nanocrystalline BaF_2 and CuO.[8,16] However, a subsequent study of the evolution of the fluorine concentration, using a fluorine-selective electrode, has shown that the composition of the fluoride phase evolves significantly during the thermal cycle.[17] Concomitantly with such evolution, CuO particles coarsen (at a rate which depends on $P(H_2O)$[18]) and Y_2O_3 and $Y_2Cu_2O_5$ particles appear within the fluoride matrix. Therefore the reaction leading to epitaxial YBCO does not occur within a homogeneous mixture of phases in physical contact but among grains separated by tens of nanometers dispersed in the bulk of an oxyfluoride matrix having the fluorite structure and variable composition which simultaneously provides Ba (solute) and acts as the solvent. Obviously, in this scenario understanding the behavior of the fluorite-type solvent is essential to understanding the growth mechanism of YBCO. In particular, the above mentioned fluorine selective electrode measurements,[17] indicated that the F/Ba ratio evolves from 2.7 to 1.5 with increasing temperature before any evidence for the formation of YBCO thus signaling that there is no single reaction describing the whole process. According to the $BaF_2 - YF_3$ phase diagram,[19,20] the trajectory followed by the F/Ba ratio between 350 and 550 °C is consistent with the variation of the solid solubility of Y in BaF_2. This is especially relevant because it has been determined that for certain compositions, mixtures of CuO with Ba−Y oxyfluorides may exhibit partial melting within the range of 500−600 °C,[17,21] i.e., below the nucleation temperature of YBCO. Though no direct microstructural fingerprints of partial melting within the bulk oxyfluoride matrix have been detected in the present study, it has been argued that the high density and sharp texture achieved by the ex situ TFA route are indicative of a liquid-mediated growth.[22]

As far as the nucleation mechanism is concerned, it has been long recognized that YBCO nucleates exclusively on the buried substrate surface. To the authors' knowledge, there is no accurate determination of the nucleation temperature, but X-ray diffraction studies of samples quenched from intermediate temperatures show first fingerprints of YBCO at ∼700 °C.[17,21] That means that the precursor film undergoes severe transformations prior to YBCO nucleation, involving the formation of transient oxide phases in the bulk oxyfluoride matrix, like Y_2O_3 and, most significantly, $Y_2Cu_2O_5$, which also nucleates at ∼700 °C.[21] Therefore, the nucleation and growth of epitaxial YBCO can occur simultaneously with "homogeneous" nucleation and growth of $Y_2Cu_2O_5$. An early detailed TEM study of quenched YBCO samples prepared by physical vapor deposition (PVD) on STO substrates[23,24] showed that a heteroepitaxial (111)-oriented oxyfluoride containing Y, Ba, F, and O constitutes low-barrier nucleation sites, in a way that the fluorite (111) planes become the (001) ones of the YBCO film. Those authors also observed an ∼7 nm thick amorphous layer at the growth front of YBCO islands that were considered to correspond to a liquid phase at 735 °C. Such an amorphous layer assisting the growth of YBCO has been reported by some authors[23−26] and, taking into account the high sensitivity of the melting temperature of the oxyfluoride phase to composition, its formation could be favored by the development of concentration gradients ahead of the growth front. However, there is no evidence that the growth of YBCO from the solid precursor is always assisted by an interfacial liquid layer.

As modeled by Honjo et al.,[27] the $[P(H_2O)]^{1/2}$ dependence of the YBCO growth rate supports the idea that the conversion process is controlled by transport in the gas phase. In particular, those authors conclude that the growth rate is limited by mass transport across a gas boundary layer located at the precursor−gas interphase, rather than by the mass transport across the YBCO growth front. As a microstructural consequence of this thermodynamic behavior, it appears that partially reacted films may exhibit marked variations of the extent of the conversion process with position on the substrate. Furthermore, given the complexity of the precursor evolution, presumably there is not a unique microstructural scenario for the nucleation and growth of YBCO, in contrast with views provided by previous reports on transmission electron microscopy studies of partially reacted samples.

(11) McIntyre, P. C.; Cima, M. J.; Ng, M. F. *J. Appl. Phys.* **1990**, *68*, 4183.
(12) McIntyre, P. C.; Cima, M. J.; Smith, J. A.; Hallock, R. B.; Siegal, M. P.; Phillips, J. M. *J. Appl. Phys.* **1992**, *71*, 1868.
(13) Karmanenko, S. F. *Supercond. Sci. Technol.* **1999**, *12*, 36.
(14) Solovyov, V. F.; Wiessmann, H. J.; Wu, L.; Zhu, Y.; Suenaga, M. *IEEE Trans. Appl. Supercond.* **2001**, *11*, 2939.
(15) Puig, T.; González, J. C.; Pomar, A.; Mestres, N.; Castaño, O.; Coll, M.; Gàzquez, J.; Sandiumenge, F.; Piñol, S.; Obradors, X. *Supercond. Sci. Technol.* **2005**, *18*, 1141.
(16) Shibata, J.; Honjo, T.; Fuji, H.; Araki, T.; Hirabayashi, I.; Hirayama, T.; Izumi, T.; Shiohara, Y.; Yamamoto, T.; Ikuhara, Y. *J. Mater. Res.* **2002**, *17*, 1266.
(17) Yoshizumi, M.; Seleznev, I.; Cima, M. J. *Physica C* **2004**, *403*, 191.
(18) Takeshi, A.; Hirabayashi, I.; Shibata, J.; Ikuhara, Y. *Supercond. Sci. Technol.* **2002**, *15*, 913.
(19) Sobolev, B. P.; Ippolitov, E. G.; Zhigarnovski, B. M.; Garashina, L. S. *Inorg. Mater.* **1965**, *1*, 334.
(20) Sobolev, B. P.; Tkachenko, N. L. *J. Less-Common Met.* **1982**, *85*, 155.
(21) Wong-Ng, W.; Cook, L. P.; Suh, J.; Levin, I.; Vaudin, M.; Feenstra, R.; Cline, J. P. *Mater. Res. Soc. Symp. Proc.* **2002**, *689*, 337.
(22) Holesinger, T. G.; Arendt, P. N.; Feenstra, R.; Gapud, A. A.; Specht, E. D.; Feldmann, D. M.; Larbalestier, D. C. *J. Mater. Res.* **2005**, *20*, 1216.
(23) Wu, L.; Zhu, Y.; Solovyov, V. F.; Wiesmann, H. J.; Moodenbough, A. R.; Sabatini, R. L.; Suenaga, M. *J. Mater. Res.* **2001**, *16*, 2869.
(24) Wu, L.; Solovyov, V. F.; Wiesmann, H. J.; Zhu, Y.; Suenaga, M. *Appl. Phys. Lett.* **2002**, *80*, 419.
(25) Teranishi, R.; Fuji, H.; Honjo, T.; Nakamura, Y.; Izumi, T.; Shiohara, Y.; Shibata, J.; Yamamoto, T.; Ikuhara, Y.; Yoshimura, M. *Physica C* **2002**, *378−381* 1033.
(26) Shibata, J.; Honjo, T.; Fuji, H.; Teranishi, R.; Izumi, T.; Shiohara, Y.; Yamamoto, T.; Ikuhara, Y. *Physica C* **2002**, *378−381*, 1039.
(27) Honjo, T.; Nakamura, Y.; Teranishi, R.; Fuji, H.; Shibata, J.; Izumi, T.; Shiohara, Y. *IEEE Trans. Appl. Supercond.* **2003**, *13*, 2516.

With the aim to provide an overall appreciation of the conversion process, the present work addresses both the phase evolution within the precursor, prior to YBCO nucleation, and the nucleation mechanism of YBCO, using transmission electron microscopy.

Experimental Section

Solution Preparation. TFA solutions were prepared following a modified procedure.[28] YBCO commercial powder was dissolved in a stoichiometric quantity of trifluoroacetic anhydride and a small quantity of trifluoroacetic acid (used as a catalyst) in acetone. The resulting solution was refined by evaporation under vacuum to yield a glassy green residue. This residue was then dissolved in methanol to give a final anhydrous solution with an ion metal concentration of 1.5 mol/L.

Substrate Preparation and Solution Deposition. The gel films were deposited on commercial 5 mm × 5 mm (00l)-oriented $LaAlO_3$ (LAO) single-crystal substrates by spin coating. Substrates were cleaned in successive ultrasonic baths in acetone and methyl alcohol, followed by a final drying step in pure N_2 gas. Spin coating was performed at approximately 6000 rpm for 2 min using an acceleration time of 1 s. The coating was performed at ambient temperature in the range of 20−22 °C and relative humidity in the range of 19−24%.

Growth of Films. The standard growth process used in the present investigation has been reported elsewhere.[15] In brief, it consists of a pyrolysis step, which is carried out under a wet oxygen atmosphere, in order to avoid any sublimation of $Cu(TFA)_2$. This stage favors the burning of the organic content of the precursor. Then the sample is submitted to a high-temperature (795 °C) firing step in an atmospheric mixture of N_2, O_2 (200 ppm), and H_2O (P_{H2O} = 0.6 kPa) under a gas flow of 0.61 L/min to form the YBCO phase. Finally, films are oxygenated at 450 °C under a flow of O_2 for 3.5 h to obtain the superconducting phase. Pyrolyzed films were placed in a furnace and quenched immediately after reaching the target temperatures.

Structural Characterization. X-ray diffraction analysis (XRD) was performed on as-pyrolyzed films and films quenched from different temperatures to obtain information on their phase content and characterize their texture. μ-Raman spectroscopy was also used as a complementary tool for phase identification. The microstructure and local chemical composition of the samples were further characterized by cross-sectional transmission electron microscopy (XTEM) using the Philips CM20 and Jeol 2010 FEG electron microscopes, both operated at 200 kV and equipped with a Gatan Image Filter 200 EELS spectrometer with an energy resolution of 0.8 eV. Elemental maps were obtained with a Philips Technai STEM microscope equipped with EDX, operated at 200 kV. Thin foils for XTEM observation were prepared by the conventional cutting, gluing, and grinding procedures, followed by a final milling step with Ar ions down to perforation.

Results and Discussion

Phase Evolution of the Precursor Film. Figure 1 shows a series of $\theta-2\theta$ scans of precursor films quenched from different temperatures. After the pyrolysis, the patterns exhibit only broad features, consistent with the nanocrystalline nature of the films, which were identified as $Ba_{1-x}Y_xF_{2+x}$ (BYF)[20] and CuO. The present data does not allow us to univocally rule out the presence of Y_2O_3. The most intense reflection of Y_2O_3, the (222) one, appears around $2\theta \sim 29°$ and therefore would be masked by the (002) BYF reflection. Since Y_2O_3 is an active Raman compound, the samples were further characterized using μ-Raman spectroscopy. No signatures of Y_2O_3 were found in the pyrolyzed films, thus suggesting that after the pyrolysis, at least a large fraction of the Y content in the precursor film is integrated in the BYF solid solution. According to experimental phase diagram studies, the extension of this solid solution is limited, $x = 0.35$ being the richest Y composition compatible with the fluorite structure.[20] This composition corresponds to a Y/Ba atomic ratio of 0.54, close to that introduced in the precursor solution. Therefore, the BYF solid solution can accommodate the initial Y/Ba ratio. The BYF lattice parameter, estimated from $\theta-2\theta$ scans, is 6.04 Å corresponding to $x = 0.28$, i.e., Y/Ba = 0.38, and according to the nominal stoichiometry, F/Ba = 2.4, in agreement with the value of 2.7 estimated by Yoshizumi et al. from selective electrode measurements.[17] In the estimation of the Y concentration in the BYF solid solution, we have neglected the influence of oxygen on the lattice parameters. Owing, on the one hand, to the similarity between the ionic radius of oxygen and fluorine anions in a tetrahedral environment (0.124 and 0.117 nm, respectively[29]) and the dissimilarity between those corresponding to Ba^{2+} and Y^{3+} in octahedral coordination (0.149 and 0.104 nm, respectively[29]), a partial substitution of F by O should have, to a first approximation, little influence on the variation of the lattice constants.

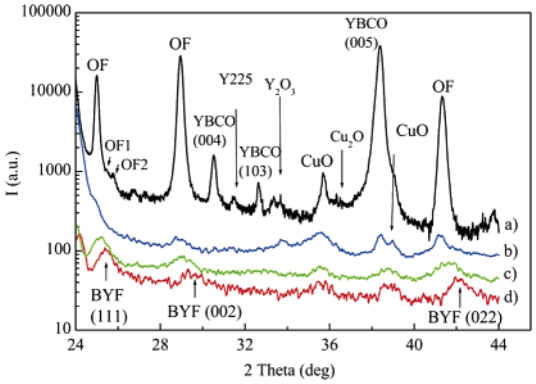

Figure 1. X-ray diffraction patterns of films (a) quenched from 795 °C, (b) quenched from 700 °C, (c) quenched from 600 °C, and (d) as-pyrolyzed. Y225, OF, and BYF stand for $Y_2Cu_2O_5$, oxyfluoride, and $Ba_{1-x}Y_xF_{2+x}$, respectively. OF1 corresponds to the (030) reflection of the ordered oxyfluoride, and OF2 is associated with a Y-enriched BYF solid solution found around growing YBCO islands (see the text).

Therefore, although most of the Y present in the pyrolyzed film is contained in the BYF solid solution, some amount of free Y_2O_3 may be present, which probably remains silent to XRD and μ-Raman spectra due to its nanocrystalline or even amorphous nature. Samples quenched from 795 °C exhibit sharp (00l) YBCO reflections (in addition to the (103) one, indicative of a small fraction of disoriented YBCO), as well as unreacted BaF_2, BYF, $Y_2Cu_2O_5$, Y_2O_3, and CuO (Figure 1). The origin of the two peaks appearing at $2\theta \sim 25.5°$ and 25.8° (indicated by OF1 and OF2) is discussed below.

(28) Romà, N.; Morlens, S.; Zalamova, K.; Ricart, S.; Moretó, J. M.; Pomar, A.; Puig, T.; Obradors, X. *Supercond. Sci. Technol.* **2006**, *19*, 521.

(29) Shannon, R. D. *Acta Crystallogr., Sect. A* **1976**, *32*, 751.

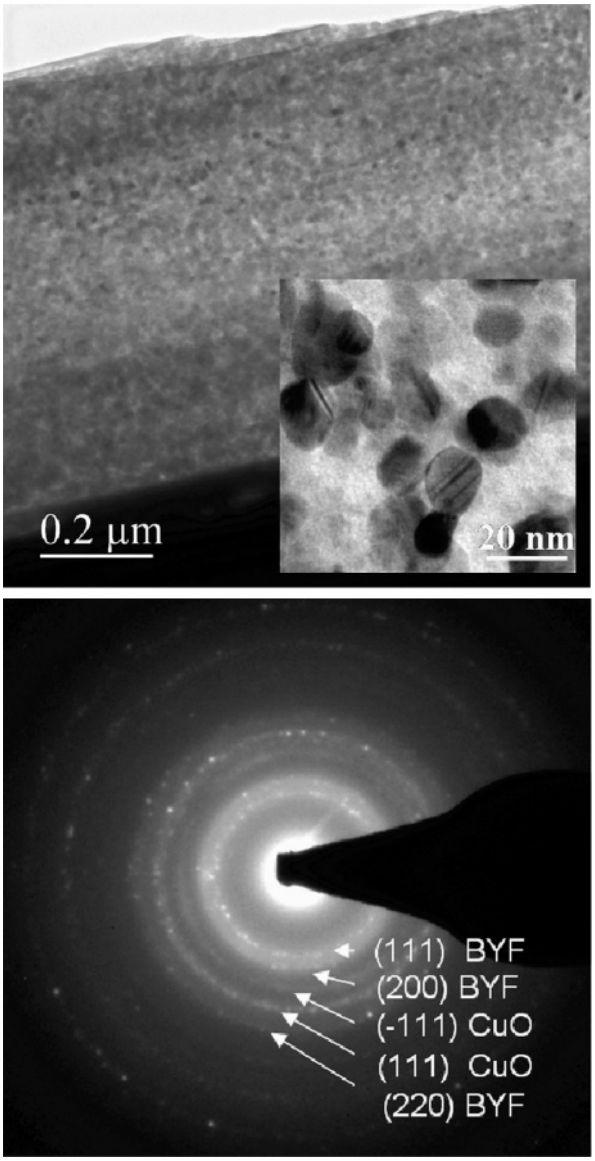

Figure 2. (a) Low-magnification XTEM image of an as-pyrolyzed film. The precursor forms a homogeneous, 800 nm thick film, nanostructured, and partially amorphous fluoride matrix of composition $Ba_{1-x}Y_xF_{2+x}$ (see the text), with embedded CuO nanoparticles. The inset is a higher magnification XTEM image to illustrate the size and shape of the CuO particles. (b) Corresponding selected-area diffraction pattern.

Figure 2a is a low-magnification XTEM image corresponding to a pyrolyzed 800 nm thick film. The speckled contrast is due to CuO nanoparticles, shown at a higher magnification in the inset. Figure 2b shows the corresponding selected-area electron diffraction pattern, which, in agreement with the analysis of the $\theta-2\theta$ scans reported in the preceding paragraph, can be indexed with the BYF and CuO phases. In agreement with phase diagram studies,[20] Figure 1 shows that increasing the temperature decreases the Y content of the BYF solid solution. Simultaneously, the intensity corresponding to BaF_2 and Y_2O_3 increases, while part of that Y_2O_3 reacts with CuO yielding $Y_2Cu_2O_5$. EELS analyses of a sample quenched from 795 °C indicate that the fluoride phase contains oxygen, while the peak corresponding to F is systematically very weak (Figure 3). Though the F peak may be weakened as a result of F loss during e-beam irradiation in the electron microscope, and therefore intensity

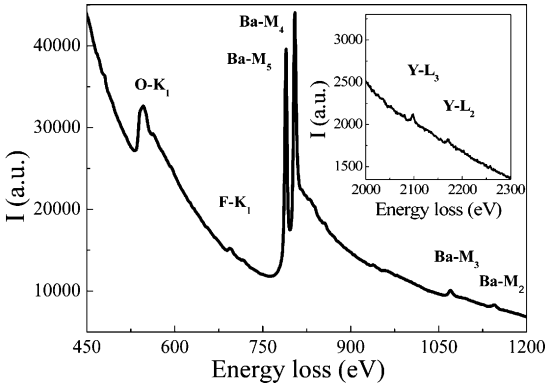

Figure 3. EELS spectrum obtained from the OF matrix in a sample quenched from 795 °C. The inset shows a higher energy region to check the occurrence of Y.

ratios cannot be used to quantify the degree of oxidation, the oxygen peak shown in Figure 3 is consistent with a substantial degree of substitution of F by O ions, as suggested previously.[23,30] At higher energy losses, the EELS spectrum also exhibits weak signatures of Y (see the inset). In the following this phase will be referred to as oxyfluoride (OF), while the acronym BYF will be used for the $Ba_{1-x}Y_xF_{2+x}$ solid solution regardless its degree of oxidation.

The observed phase evolution agrees with the trajectory of the F/Ba ratio previous to YBCO nucleation, reported by Yoshizumi et al.[17] According to those authors, the F/Ba ratio evolves from 2.7 at 350 °C to 1.5 at 700 °C, F/Ba = 2 (corresponding to BaF_2) being achieved at 550 °C. For F/Ba > 2, this behavior is explained by the formation of the BYF solid solution and the temperature dependence of the Y solid solubility in BaF_2. Unfortunately, as a result of the high density of embedded CuO nanoparticles, EELS analyses performed on the as-pyrolyzed BYF did not yield reliable results concerning its degree of oxidation. However, the trajectory reported for the F/Ba ratio suggests that the oxygen content of the fluoride phase is presumably small below 500 °C.[17] In order to explain the trajectory between ratios 2 and 1.7, Yoshizumi et al.[17] suggest the expected reaction $BaF_2 + H_2O \rightarrow BaO + 2HF(g)$. However, we have not detected significant fingerprints of BaO, thus signaling that this reaction does not occur to a significant extent during the conversion to YBCO, in contrast with that originally expected. These considerations are, moreover, in agreement with the topotactic character of the YBCO conversion mechanism, where YBCO is formed as a result of the insertion and replacement of chemical species in the fluorite structure,[23,24] resulting in a severe structural modification, as opposed to the simpler chemical reaction between grains in direct physical contact. Therefore, the drop of the F/Ba ratio below 2 is more likely associated with the replacement of F by O in the fluorite structure, in agreement with the strong oxygen signal appearing in the EELS spectrum (Figure 3).

The behavior discussed in the preceding paragraph emphasizes the role played by the fluorite-type matrix (either fluoride or oxyfluoride) as a solvent, i.e., its ability to

(30) List, F. A.; Specht, E. D.; Heatherly, L.; Leonard, K. J.; Sathyamurthy, S.; Kroeger, D. M. *Physica C* **2003**, *391*, 350.

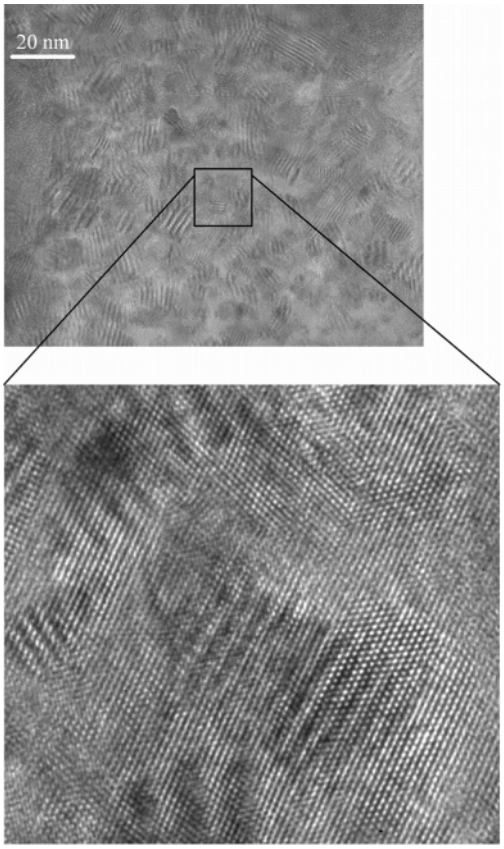

Figure 4. Low- and high-magnification high-resolution XTEM images of the OF matrix quenched from 795 °C. Images are viewed along [110].

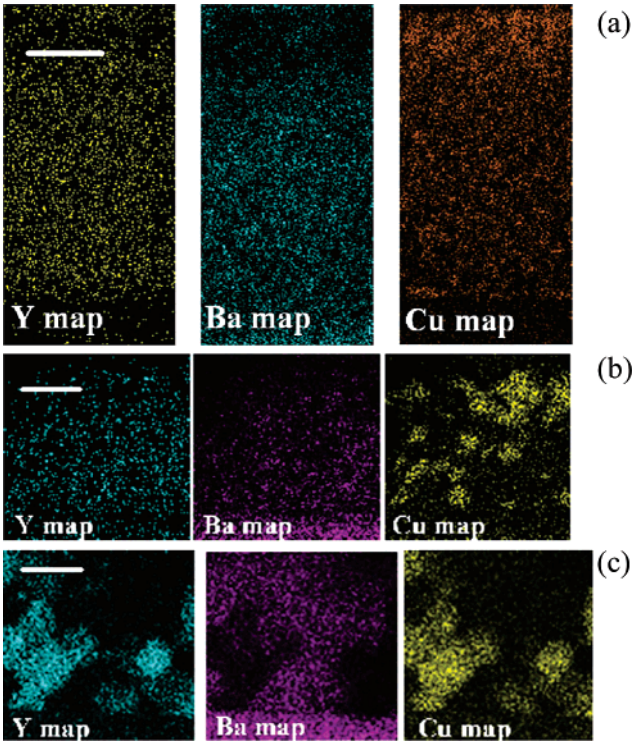

Figure 5. Cross-sectional STEM EDAX Cu, Ba, Y, and O elemental maps of samples quenched from (a) 600 °C, (b) 700 °C, and (c) 795 °C. The scale bar corresponds to 200 nm.

accommodate important compositional variations. It has been reported that the melting point (T_m) of the fluoride phase is strongly sensitive to the Y and O content. In particular, T_m drops down within the 500−600 °C range in the BaF_2−CuO−Y(O, F) region, corresponding to F/Ba > 2.[17,21] This observation has led to the argument that the growth of YBCO is assisted by the formation of a partial melt. However, as discussed above, low melting point F/Ba > 2 compositions would appear at relatively low temperatures, i.e., below ∼550 °C, and there is no evidence that samples are submitted at temperatures higher than T_m at any stage. The unique microstructural feature reported so far that supports partial melting is the occurrence of an amorphous layer, a few nanometers thick, at the precursor−YBCO interface.[23−26] Although melting at the growth front might result from the development of concentration gradients favoring low melting point compositions ahead of the growth front, such an amorphous layer has not been detected in the course of the present investigation, thus signaling that formation of interfacial liquids is not essential for the growth of YBCO. On the other hand, as far as the bulk OF matrix is concerned, it is interesting to note that its nanostructured character is deduced from the extended occurrence of Moiré contrasts, indicative of the superposition of nanometric crystalline domains, as well as lattice contrast variations, rather than the identification of grain boundaries in high-resolution XTEM images. This is clearly illustrated in Figure 4. Most strikingly, the orientation of the nanocrystals building such a nanostructured framework is kept unchanged through several tens, even a few hundred, of nanometers, thus suggesting that XTEM images in fact constitute snapshots of a rapidly varying microstructure evolved from an epitaxial configuration. The resulting mosaicity is then likely to result from the accommodation of internal stresses associated with the chemical evolution of the BYF solid solution. Note that partial melting would very likely induce amorphization at grain boundaries of such a mosaic substructure, thus emphasizing the subboundary network, which is not observed. Therefore, though very likely the OF precursor is submitted at temperatures close to T_m, thus enhancing diffusive processes, no definitive traces of partial melting can be identified in the present samples.

Segregation of Phases. Elemental distribution maps of films quenched from different temperatures were obtained by X-ray energy-dispersive analysis using a scanning transmission imaging mode (STEM). Spatial cation distributions reveal that the complex phase evolution discussed in the preceding section is accompanied by a strong cationic segregation. Figure 5a−c shows the cross section Y, Ba, and Cu maps corresponding to samples quenched from 600, 700, and 795 °C, respectively. It can be observed that, at 600 °C (Figure 5a), Cu exhibits a concentration gradient perpendicular to the interface, exhibiting higher values toward the upper part of the film, while Y and Ba show an inverse trend. As the temperature is raised, the overall cation distribution is progressively homogenized, though short-scale heterogeneities appear at 700 °C as a result of grain growth (Figure 5b). Note that at 700 °C first fingerprints of YBCO (00*l*) reflections appear in the XRD patterns (Figure 1). Such heterogeneities grow in size up to ∼200 nm when the temperature reaches 795 °C (Figure 5c). A striking feature of Figure 5c is the close correspondence between the Cu and Y maps (a differential feature is arrowed in the Y map).

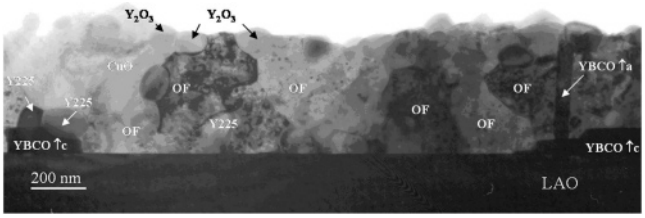

Figure 6. Low-magnification XTEM image of the film quenched from 795 °C observed from [100]LAO. Phases identified from EELS analyses performed at some points of the specimen are indicated. The *c*-axis-oriented YBCO islands with a thickness of 80−90 nm are observed. An *a*-axis-oriented YBCO grain is also shown on top of an island.

Such a striking correspondence, along with the absence of Ba in the Y−Cu-rich areas, points to the formation of large grains of $Y_2Cu_2O_5$ within the OF matrix. Significantly, mappings in this area do not show any evidence of YBCO formation, which suggests the existence of a thermal window within which bulk nucleation of $Y_2Cu_2O_5$ and epitaxial YBCO are competitive processes.

Figure 6 is a low-magnification XTEM image of the film quenched from 795 °C, viewed along the [100]LAO direction. In order to get a rough view of the distribution of phases, results of EELS analyses performed at some points of the cross section are indicated in the image. In agreement with EDX mapping, Figure 6 reveals pronounced phase segregation. YBCO islands are shown to nucleate exclusively on the substrate surface, preferentially with their *c*-axis perpendicular to it. It is worth mentioning that despite the fact that the islands shown in the image have already grown to a significant thickness (50−100 nm), the distance between them is still notably large, ∼1 μm, indicating an initial anomalously large nucleation spacing (this extreme will be further considered below). An *a*-axis-oriented YBCO grain reaching the film surface, nucleated on top of a *c*-oriented island, can also be observed. The film exhibits, at this stage of the growth process, approximately half of the precursor film thickness, i.e., 450 nm, while after the complete process the film thickness will further reduce down to 300 nm. Therefore, such *a*-axis grains will outcrop on the flat *c*-axis-oriented surface. Overall, the image reveals that at 795 °C the OF phase constitutes a homogeneous matrix containing, $Y_2Cu_2O_5$, CuO, and Y_2O_3 grains, besides YBCO.

Careful inspection of the XRD pattern of the 795 °C sample in Figure 1 also shows a shoulder between the CuO and (005)YBCO peaks, that can be attributed to the (111) reflection of Cu_2O. Interestingly, a careful observation of Cu−O-rich areas in the XTEM images signaled the coexistence of two phases, one very fine grained and another one exhibiting well-developed grains. EELS spectra obtained from both phases, shown in Figure 7, exhibit distinctive features characteristic of Cu_2O for the nanocrystalline phase and CuO for the coarse-grained one. In particular, that corresponding to Cu_2O can be distinguished by a slight shift toward higher energy losses. Unlike PVD-derived films, in which Cu is in the form of Cu_2O up to 500−700 °C,[23,31] the pyrolysis step required in the TFA route favors the formation of CuO. The Cu_2O−CuO boundary is close to 700 °C at the

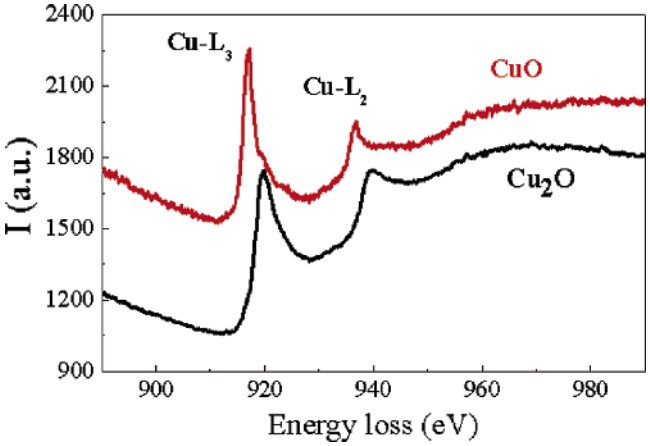

Figure 7. EELS spectra obtained from the nanocrystalline and coarse-grained regions of a Cu−O-rich area, revealing the L-Cu peaks of Cu_2O and CuO, respectively (see the text).

growth conditions ($pO_2 \sim 2 \times 10^{-4}$ atm), and therefore the observation of Cu_2O might be attributed to a partial reduction of CuO during heating to the growth temperature (795 °C).[32] However, the present results do not permit us to draw conclusions on either the statistical relevance of this observation or on its role on the precursor conversion process.

Turning to the issue of YBCO versus $Y_2Cu_2O_5$ competitive growth, let us focus back on Figure 6. There is a YBCO island located close to the left-hand edge of the image, which supports two $Y_2Cu_2O_5$ grains on its top. Note that the growth of the island is clearly impeded by the two grains, particularly that located on the right-hand side. High-temperature in situ XRD experiments of e-beam evaporated TFA precursors have revealed that the $Y_2O_3 + 2CuO \rightarrow Y_2Cu_2O_5$ reaction takes place at ∼700 °C,[31] thus indicating that $Y_2Cu_2O_5$ and YBCO nucleate at very close temperatures. Our observations in fact reveal that the nucleation and growth of YBCO is assisted by long-range diffusion within a barium oxyfluoride matrix rather than interphase reaction among the different phases. Hence, the conversion of the precursor to YBCO does not necessarily require the formation of $Y_2Cu_2O_5$, but its formation, though unavoidable under the present conditions, may even slow down the kinetics of the transformation to YBCO, with important implications from the industrial production point of view. Interestingly, Wong-Ng et al. reported for PVD-derived samples that YBCO films can be obtained without the formation of $Y_2Cu_2O_5$ when ($BaF_2 + YF_3 + Cu$) precursors are used.[31] Though in that particular case the reaction was incomplete at the end of a standard process, this finding demonstrates that the microstructural scenario for the conversion to YBCO can be dramatically modified through a proper choice of the precursor materials. This is an interesting extreme deserving further attention.

As a further manifestation of phase segregation we consider here the ordering within the OF phase. High-resolution XTEM images of the OF matrix featured fingerprints of atomic ordering, either within nanometric domains embedded in the OF (Figure 8), or within larger domains surrounding some heteroepitaxial YBCO islands, as shown

(31) Wong-Ng, W.; Levin, I.; Feenstra, R.; Cook, L.; Vaudin, M. *Supercond. Sci. Technol.* **2004**, *17*, S548.

(32) Maffott, W. G. *Handbook of Binary Phase Diagrams*; Genium: Schenectady, NY, 1984−1999.

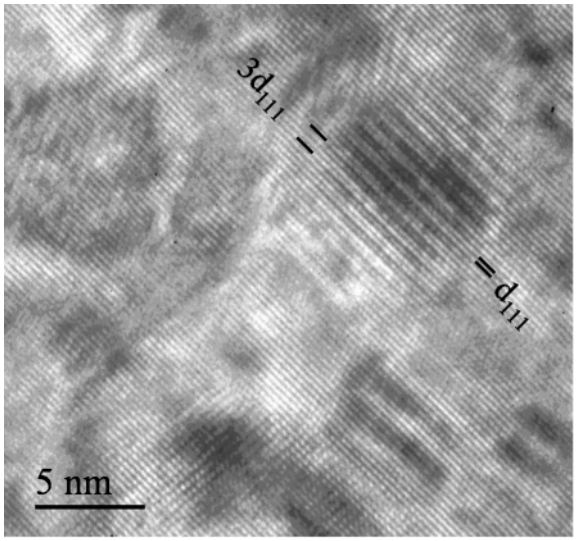

Figure 8. High-resolution XTEM image evidencing atomic ordering within a nanometric domain embedded in the OF matrix. The arrowed domain exhibits a tripled $d_{(111)}$ spacing.

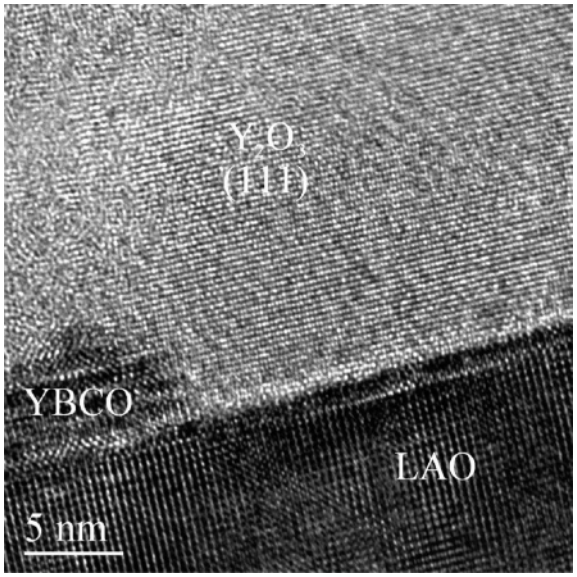

Figure 9. High-resolution XTEM image of a YBCO nucleus embedded in a (111)-oriented Y_2O_3 grain.

below. Figure 8 shows such an ordered domain, characterized by a triple $d_{(111)}$ spacing of the corresponding OF phase. The formation of this phase is important because it has been suggested to constitute a template for the nucleation of YBCO.[23,24] It has been found that there is not a unique way to order the OF phase,[23,24] and it is likely that a series of related OF-based superstructures exists. Among these, that reported by Wong-Ng et al.[31] has lattice parameters of $a = 0.74$ nm, $b = 1.05$ nm, and $c = 0.43$ nm (in this setting, the [010] direction of the superstructure is taken along the [111] direction of the OF fluorite-type structure). Note that the $d_{(111)}$ spacing of the fluorite structure is tripled as result of ordering. Thus, the peak marked as OF1 in Figure 1, appearing at $2\theta \sim 25.5°$, can tentatively be attributed to the (030) peak of the ordered OF.

Texture of Precursor Phases, Nucleation and Growth Mechanism of YBCO. As discussed above, the BYF solid solution evolves to the OF-type phase on heating up to the growth temperature at 795 °C. During this process, Y_2O_3 forms which can either react with CuO to form $Y_2Cu_2O_5$, nucleate within the bulk OF phase, or nucleate heteroepitaxially on the substrate surface. Figure 9 is a high-resolution XTEM image, viewed along the <100>LAO direction, showing a heteroepitaxially nucleated ~3 unit cell YBCO island embedded in a Y_2O_3 matrix. The epitaxial relation between the Y_2O_3 and the LAO substrate is $(111)Y_2O_3$//(001)LAO, $[-1,2,-1]Y_2O_3$//[100]LAO.

In order to obtain an average picture of the texture of the fluoride phase in a sample quenched from 795 °C, a pole-figure was recorded for a 2θ value of 41.1°, which corresponds to the (202) reflection of the OF phase and the (111) reflection of the LAO substrate. The resulting pole-figure, shown in Figure 10a, exhibits the four equivalent {111} LAO poles at an inclination $\chi = 54.7°$, providing the in-plane orientation of the substrate for reference. Decreasing the inclination to the substrate normal, one first finds four poles at $\chi = 45°$, corresponding to the {202} planes of the (001)-oriented OF (hereafter denoted as $\{202\}OF^{<001>}$). The coincidence in azimuth (ϕ) between the {202} poles and the

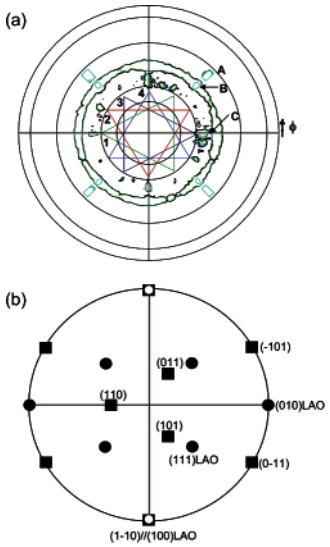

Figure 10. (a) Pole-figure corresponding to the (202) OF and (111) LAO reflections (A:{111}LAO, B:$\{202\}OF^{<001>}$, C:$\{202\}OF^{<111>}$, see the text) and (b) stereographic projection of the {100}LAO and {220}OF poles, viewed along the [001]LAO and [111]OF directions, respectively.

{111} poles of LAO is consistent with an epitaxial orientation relationship given by $(001)OF^{<001>}$//(001)LAO, $[110]OF^{<001>}$//[100]LAO. Note, however, that these poles appear superposed to a ring of intensity which tells us that a significant fraction of (001)-oriented OF exhibits uniaxial texture. Taking $a_{OF} = 0.62$ nm, this fraction of in-plane disordered material can be interpreted as resulting from the high mismatch strain with the LAO substrate ($a_{LAO} = 0.379$ nm): $\epsilon \sim 13\%$. Finally, we find weak discrete peaks scattered at $\chi \sim 35°$. This intensity corresponds to the {220}-type poles associated with the (111)-oriented OF. Careful inspection reveals that the maxima are not randomly distributed, but most of them are located at the vertices of four equilateral triangles rotated 30° one to each other. In order to understand the in-plane orientation which is derived from this pole arrangement, Figure 10b shows the stereographic projection of the {100}LAO and {220}OF poles, viewed along the [001]LAO and [111]OF directions, respec-

tively. In the cubic system, there are 12 {110} equivalent planes or poles: three are inclined 35° to [111], their inverse counterparts (not shown), and six poles lie on the equator, separated 60° to each other. The latter six ones lie on the interface plane and therefore define three equivalent matching directions with the substrate (Figure 10b). Comparison of parts a and b of Figure 10 reveals that the four triangles identified in the pole-figure correspond to six ways to align <110>OF with <100>LAO on the interface plane, namely, [−1,1,0]OF, [−1,0,1]OF, and [0,1,−1]OF can align either with [100]LAO or [010]LAO. Note that a 180° rotation leaves the configuration unchanged. Hence triangles 1 and 3, and 2 and 4, as indicated in Figure 10a, correspond to equivalent orientations. On the other hand, each triangle may correspond to three different in-plane orientations each obtained through a 120° rotation around the substrate normal. The six nonequivalent in-plane orientations are then obtained considering the three different possible orientations associated with each of the two independent triangles (e.g., 1 and 2).

As a result of the ternary symmetry of the [111] projection, each in-plane orientation only has one matching direction (<110>OF with <100>LAO, as found for the (001)OF orientation), and therefore, owing to interfacial energy considerations, (111)-oriented OF nuclei would be less favored than (001)-oriented ones (which carry two orthogonal <110> matching directions). These considerations would explain the strong tendency of the fluoride phase to nucleate with (001)-type orientation, as signaled by the prominent (002) peak observed in Figure 1. An estimation of the volume percentage of (111)-oriented OF using $\theta-2\theta$ scan intensities, assuming only (111)- and (001)-type orientations, in fact yields only 15%. As commented at the beginning of this section, XTEM observations have revealed the occurrence of (111)-oriented Y_2O_3 (Figure 8). Therefore, we may have overestimated the intensity of the (002) OF reflection as a result of its overlap with the (222) Y_2O_3 one. However, the observation of other, nonheterogeneously nucleated, Y_2O_3 particles far from the interface, suggests that this contribution is small. Anyway, the derived value of 15 vol % for (111)-OF is indicative of a dominant population of (001)-oriented OF consistent with interfacial structure considerations.

As shown in the previous section, the OF phase is prone to develop ordered structures, whose main fingerprint is the tripling of the (111) spacing of the basic fluorite structure. Owing to the similarity of $3d_{(111)}$OF ∼ $d_{(001)}$YBCO, it has been argued that such ordering has a templating effect facilitating the growth of *c*-axis-oriented YBCO. The correspondence between both structures is clearly illustrated by the high-resolution electron micrograph shown in Figure 11a. The image shows in detail the growth front of a (001)-oriented YBCO island expanding through a (111)-oriented ordered OF region. Other observations, however, show that the (001)-oriented growth of YBCO is not always assisted by the OF superstructure. As an example of this situation, Figure 11b is a high-resolution XTEM image of a (001)-oriented YBCO island expanding through the (111)-oriented nonordered OF matrix, thus suggesting that very likely preexisting ordering within the OF matrix is not essential for the *c*-axis-oriented nucleation of YBCO islands. In fact,

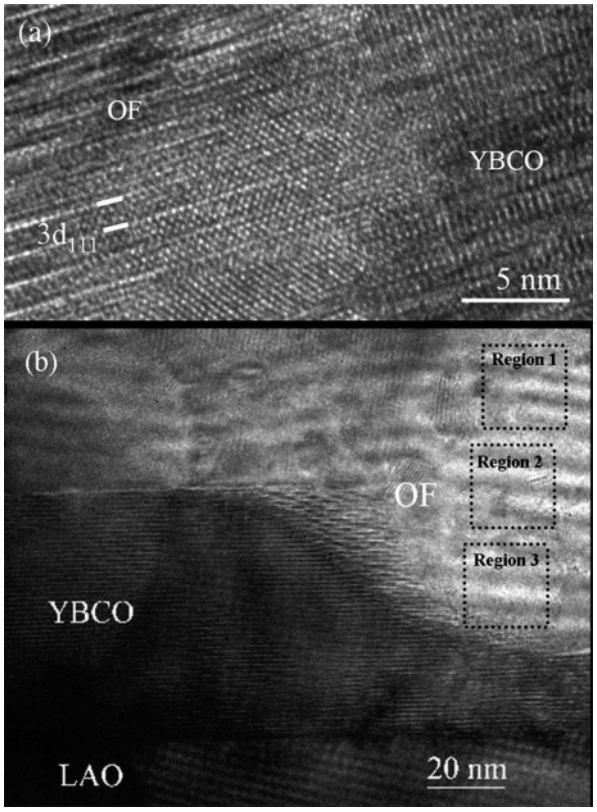

Figure 11. (a) High-resolution XTEM image of the growth front of YBCO within (111)-oriented OF exhibiting a $3d_{(111)}$ superstructure. (b) High-resolution XTEM image of the growth front of YBCO within (111)-oriented OF. Boxed areas correspond to regions used for FFT analysis of lattice parameters.

taking into account the triple stacking of perovskite units along the *c*-axis in the YBCO unit cell, in principle the templating effect of the (111)-oriented OF matrix should not depend on the occurrence of the observed superstructure.

Our observations indicate that YBCO nucleates exclusively on the substrate surface. However, in the present solid-state epitaxial process, (111)-oriented OF domains provide low-barrier nucleation sites for (001)-oriented YBCO nuclei.[23,24] Strikingly, however, our results demonstrate that almost full (001)-oriented YBCO films are obtained from precursors exhibiting only a small fraction of (111)-oriented OF. We cannot ascertain at this stage whether nucleation takes place exclusively in such an environment, or conversely, the supersaturation is too large to make nucleation sensitive to barrier differences associated with the different OF orientations. However, in the former case a relatively large internucleus distance is expected, as is indeed observed in the present samples (see Figure 6) and also reported by other authors.[33] Growth of such islands beyond the boundary of (111)-oriented OF regions should then take place through the conversion to YBCO in a different scenario, like (001)-oriented OF, without altering the initial orientation of the YBCO islands. In this situation, the initial YBCO nuclei spacing could be tuned by controlling the relative amounts of (001)- and (111)-oriented OF regions in contact with the substrate surface.

(33) Solovyov, V. F.; Wiessmann, H. J.; Suenaga, M. *Supercond. Sci. Technol.* **2005**, *18*, 239.

Turning back to Figure 11b, this image was also used to measure the lattice parameters of the OF phase around the growing YBCO, by analyzing the fast Fourier transform patterns obtained at different points of the image, as indicated by boxes. The size of the boxed areas is equivalent to the size of the transformed region. The lattice parameter obtained from region 1, at ~45 nm from the interface, $a = 0.62$ nm, corresponds to the OF phase identified in the XRD patterns. However, there is a marked decrease of the fluorite cell dimensions toward the interface: at region 2 the lattice parameter is 0.602 nm, and it drops down to 0.595 nm within a thin slab of material adjacent to the interface (region 3). Owing to the diffusive character of the precursor conversion process, such a variation of the lattice parameter around the YBCO growing island very likely reflects a concentration gradient ahead of the YBCO−OF interface. It is interesting to note that the latter value corresponds to the higher Y concentration compatible with the fluorite-type solution,[20] thus suggesting a Y concentration gradient ahead of the growth front. The weak diffraction peak marked by OF2 in Figure 1, which corresponds to a lattice spacing of 0.597 nm, can therefore be associated to this Y-enriched OF adjacent to the growth front of YBCO islands. The fact that this variation of the OF lattice parameter is reflected in the XRD $\theta-2\theta$ scans indicates that it constitutes a general feature of the OF matrix around growing YBCO domains. Since the lattice parameter $a = 0.595$ nm corresponds to a Ba/F ~ 2 ratio,[20] the present observations suggest that the OF matrix accommodates the Ba/Y stoichiometry corresponding to YBCO within a boundary layer around the growing islands and that the Y concentration rapidly decays ahead of the growth front. This behavior thus also suggests that Y supply to the growing YBCO might constitute a kinetic limiting step in the solid phase, in contrast with the current view that there is a unique growth rate-limiting process associated with mass transfer across the precursor−gas interface.[27]

Conclusions

We report a microstructural analysis of the conversion process of Y, Ba, and Cu TFA precursors to epitaxial YBCO films. After the pyrolysis step, the ceramic precursor consists of a BYF matrix with embedded CuO nanoparticles. Upon heating, the microstructural evolution of the precursor is driven by the reduction of the solid solubility of Y in the BYF solid solution. Thus, Y is released in the form of Y_2O_3, which can react with CuO to form $Y_2Cu_2O_5$. According to a previous report this reaction occurs at ~700 °C,[31] i.e., close to the YBCO nucleation temperature. At 795 °C, EELS analyses of the matrix reveal a significant oxygen content and only a weak signal of Y. This compositional evolution agrees with the previously reported F/Ba ratio trajectory, determined from fluorine-selective electrode measurements.[17] No traces of BaO are detected at any stage of the process, thus reinforcing the view that YBCO forms by a diffusive topotactic-like mechanism within the OF matrix. Although there are reports indicating that the observed compositional trajectory crosses low melting point regions,[17,21] we have not found any conclusive microstructural evidence supporting the formation of partial melts during the process.

Besides the evolution of the fluoride/oxyfluoride-type matrix, the microstructural evolution of the precursor film is characterized by coarsening of the CuO particles and the formation of $Y_2Cu_2O_5$ in the bulk matrix. In particular, the formation of this latter oxide is particularly relevant because it occurs at temperatures very close to the epitaxial nucleation of YBCO, and therefore both processes may constitute competitive phenomena thereof affecting the kinetics of the conversion process.

As indicated by early studies,[23,24] the present work supports the idea that (111)-oriented OF domains provide low-barrier nucleation sites on the buried substrate surface. Surprisingly, however, such regions only represent about 15% of the total OF matrix. Though in agreement with other studies,[33] we find direct evidence for an anomalously high internuclei spacing; it is not clear whether nucleation of YBCO is restricted to such sites. This is a major issue with implications on the grain boundary quality and distribution which deserves further attention.

Acknowledgment. This work has been supported by MEC (MAT2002-02642 and MAT2003-01584), Generalitat de Catalunya (SGR 2001-00189 and CeRMAE), and the EU (SOLSULET G5RD-CT2001-00550). A.P., J.G., and M.C. acknowledge financial support from the Spanish Ministry of Science and Education through the Ramón y Cajal, FPI and FPU programs. We also acknowledge Servei de Microscòpia Electrònica, UAB, and Serveis Científics de Barcelona, UB, for electron microscopy facilities.

CM0617891